IX. SYNOPTIC STUDIES

Application of ATS III Photographs for Determination of Dust and Cloud Velocities over the Northern Tropical Atlantic*

By Tetsuya T. Fujita

REPRINTED FROM THE JOURNAL OF THE METEOROLOGICAL SOCIETY OF JAPAN

Vol. 49, Special Issue, December, 1971

IX. SYNOPTIC STUDIES

Application of ATS III Photographs for Determination of Dust and Cloud Velocities over the Northern Tropical Atlantic*

By Tetsuya T. Fujita

The University of Chicago
(Manuscript received 23 April, 1971)

Abstract

July 14, 1969 was selected from BOMEX Period IV as the day of detailed analysis of cloud velocity fields over the northern tropical Atlantic Ocean. A total of 375 low-cloud velocities were obtained between ITCZ and 34N and 70 velocities between ITCZ and the equator. These velocities are found to be very useful in understanding circulation patterns over a vast region of water where little synoptic data is available. Over 170 high-cloud velocities were computed mostly in the area of cloud clusters. It was found that a field of high-cloud divergence existed over practically each of large cloud clusters in the ITCZ and an easterly wave appearing on this day. Motion of dust clouds from Sahara was also computed by using an accelerated movie technique. It is concluded that ATS III picture sequences can be analyzed independently from conventional synoptic and/or network data so that the computed velocities of clouds, dust, and propagating waves can be used as supplementary data to past and future tropical experiments.

1. Introduction

In view of the importance of cloud-velocity computations over the areas of past and future tropical experiments, a test analysis of cloud-motion fields over the northern tropical Atlantic was attempted. A series of ATS III global pictures taken on July 14, 1969 was selected for this purpose because BOMEX Period IV, July 11–28, 1969, was assigned for the investigation of tropical convection systems.

Assuming that the results of this test analysis could be used by those researchers who are interested in analyzing other observational data, cloud velocities were computed exclusively from a sequence of ATS pictures. After the computations of velocities no adjustments were made to fit computed velocities with observed winds. Both aerological and aircraft data were simply added to the cloud-velocity charts after their completion because cloud and wind velocities could differ considerably. The patterns of cloud velocities presented in this report should, therefore, be regarded as direct outputs from a straight computation of cloud-motion field from geostationary satellite data.

2. ESSA pictures and synoptic situations

The north Atlantic on July 14, 1969 was dominated by trade wind circulation south of the high pressure area centered at 33N and 35W with a central pressure of 1028mb.

The cloud patterns in the eastern half of the analysis area in Fig. 1 were made by joining 3 pictures from ESSA IX orbit 1727 taken respectively at 1521, 1526, and 1530 GMT, July 14, 1969. The ITCZ extended along 10N eastward to Africa. Cellular clouds within the tradewind region were seen between latitudes 15N and 30N. Faint dust clouds drifting out from Sahara were seen in the region of these cellular clouds. The leading edge of the dust clouds can be followed in the picture along a line connecting 18N & 20W, 20N & 28W, and 25N & 25W.

The western half of the analysis area shown

* The research presented in this paper was sponsored by ESSA under Grant E-198-68(G).

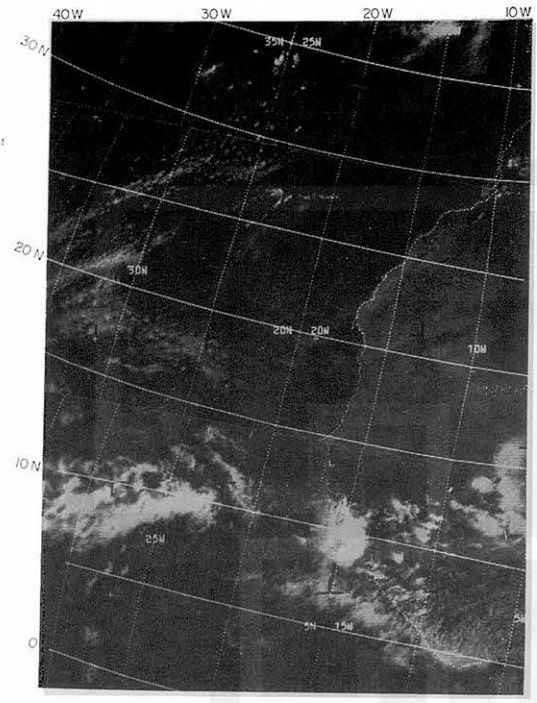

Fig. 1 ESSA IX mosaic from orbit 1727, 1521–1530 GMT, July 14, 1969, showing faint dust from Sahara drifting westward into the Atlantic. ITCZ cloud clusters are seen along 10 N latitude. Seen over the Atlantic are cellular cumuli and stratocumuli with their brightness modulated by internal gravity waves oriented in SW-NE directions.

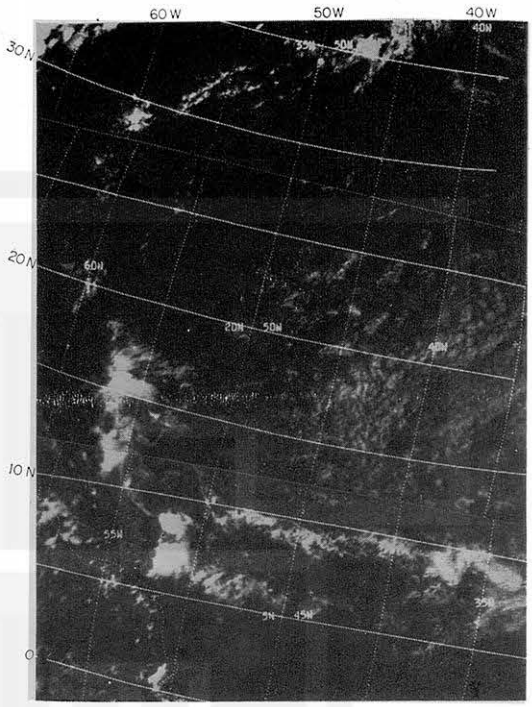

Fig. 2 ESSA IX mosaic from orbit 1728, 1716–1725 GMT, July 14, 1969, showing a weak ITCZ between 5 N and 10 N. Cloud clusters appearing along longitude 56 W are moving toward the Caribbean. Northeastern part of South America is seen near the southwest corner.

in Fig. 2 consists of 3 pictures from ESSA IX orbit 1728 exposed at 1716, 1721, and 1725 GMT, respectively. There are double bands of weak ITCZ clouds in this area. An irregular mass of cloud clusters centered near 57W & 15N was moving westward.

3. Method of cloud-velocity computation

To compute cloud displacements from ATS III pictures, 4″×5″ negatives, as listed on page II-306, ATS Meteorological Data Catalog, Vol. IV by NASA (1969), were obtained from Goddard Space Flight Center. Frames 22 through 32 with picture end times at

Picture Sequence	Picture end time (hr, min, sec)		
22	14	42	10
23	14	54	56
24	15	07	41
25	15	20	26
26	15	33	12
27	15	45	57
28	15	58	43
29	16	11	34
30	16	24	19
31	16	37	04
32	16	49	50

were selected. The time between the first and the last pictures in this sequence is 2 hr 7 min 40 sec.

Both east and west halves of the analysis area were printed separately on 8″×10″ paper so as to obtain maximum possible picture resolution out of these negatives. Shown in Figs. 3 and 4 are, respectively, the first pictures in the east and west series with a 2-deg geographic overlay grid.

After punching two registration holes on each printed picture, two film loops, one for

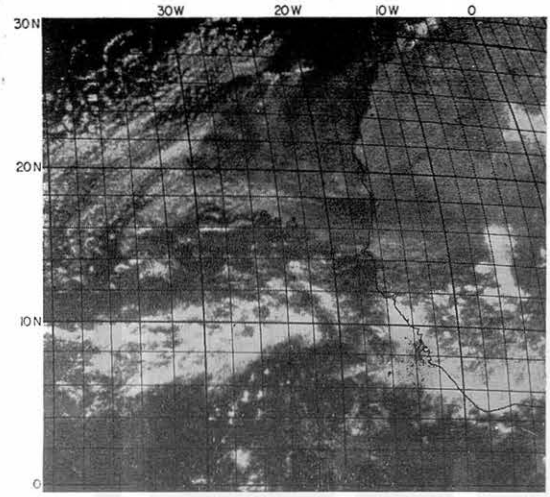

Fig. 3 Enlarged ATS III picture at 1442 Z, July 14, 1969, showing dust flow from West Africa.

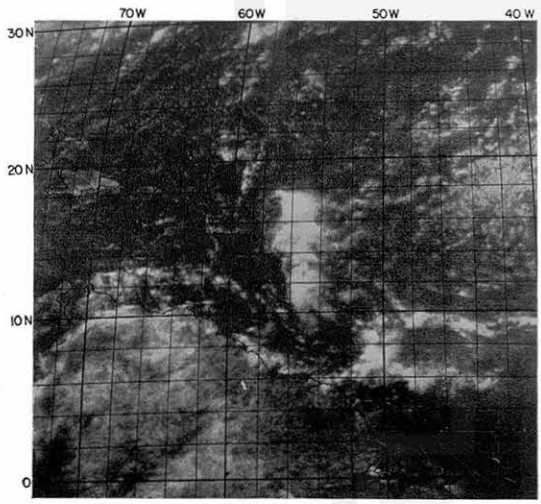

Fig. 4 Enlarged ATS III picture at 1442 Z, July 14, 1969, showing large cloud clusters to the east of Barbados.

the eastern and the other for the western areas, were made to compute displacement of clouds during this 2hr 7min 40sec period. In filming a loop, 30 frames were made of the first picture, then the following pictures were filmed 2 frames each successively, ending with 30 frames of the last picture. Then the filming order was reversed taking one frame of each picture until returning to the first picture. Then the cycle was repeated several times.

The final loops thus filmed show slow movement of clouds from their initial to the final positions. Then clouds return to their initial positions at twice the forward moving speed. On a movie screen or on a back-projection surface which was used in this analysis, cloud displacement vectors were drawn one after another until the entire field of the cloud motion was established.

Separation of cloud velocities according to the cloud heights is one of the most difficult tasks one would face in carrying out such an analysis. In this test analysis the cellular clouds which are most likely assumed to be low clouds were tracked first in order to establish a field of the low-cloud motion. If there were questionable cellular clouds, they were regarded as low clouds only when their motions fit those of nearby clouds with definite low-cloud appearances.

Fuzzy clouds, including leading edges of spreading anvils, were first assumed to be high clouds. They were, then, tracked separately from low clouds so as to determine their velocity field. It was found that the fields of motion of low and high clouds are so different that they could be mapped separately in most areas.

After obtaining vector displacements of clouds, each vector was converted into the corresponding velocity, taking into consideration the image size, the location of clouds relative to the subsatellite point, and the crossing angle. Correction diagrams for both cloud direction and speed appear in Fujita's (1969) paper.

4. Velocity of low clouds

The velocities of low clouds computed over the entire area of northern tropical Atlantic were plotted on a Mercator basemap (Fig. 5). Each wind symbol represents a cloud velocity expressed in 10kt barbs and its fraction. For instance, a 25kt velocity is given by two full and one 50%-long barbs; 13kt, by one full and one 30%-long barbs.

The velocity field analyzed with stream lines shows the existence of convergence and cyclonic vorticity characterizing the areas of ITCZ cloudiness. A similar analysis of cloud velocities over the tropical Pacific was made by Fujita, Watanabe, and Izawa (1969).

An extensive area of cloud clusters is seen to the east of West Indies, between 50 and 60

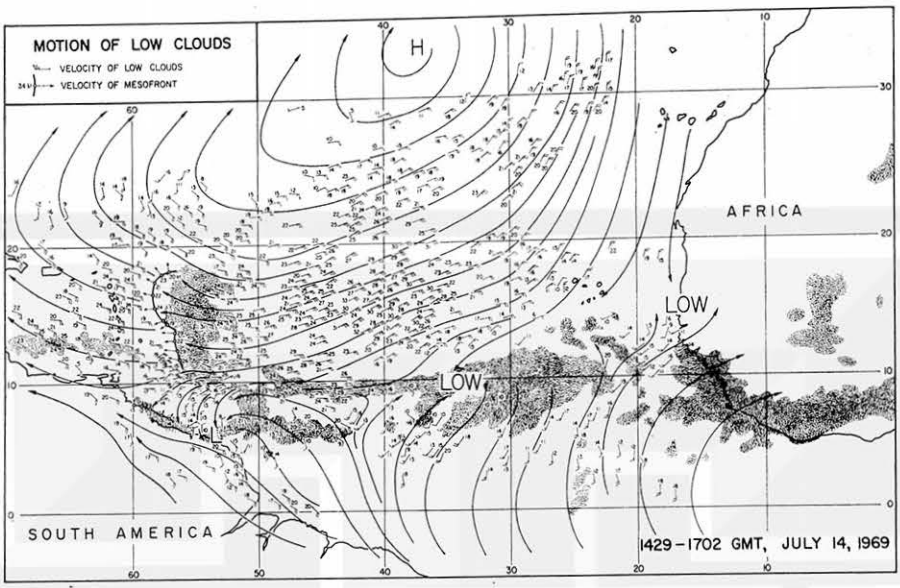

Fig. 5 Motion of low clouds computed from ATS III pictures taken between 1429–1702 Z, July 14, 1969. Stippled areas represent those of deep convection estimated through cloud analysis.

longitudes. Mean velocity of clouds east of the clusters appears to be 25 kt while that to the west of the cluster is only 12 to 18 kt, suggesting that the reduction in the velocity of cellular clouds was taking place in the area of the cloud clusters. A thin line of clouds emerging westward from these clusters appears to be very similar to the ones studied by Zipser (1969) in his analysis of ATS I pictures over the Pacific. The speeds of the line as indicated in the figure are 20 to 30 kt, implying that this line undercuts small cellular, low clouds as it travels westward. It is not feasible to determine the exact area and

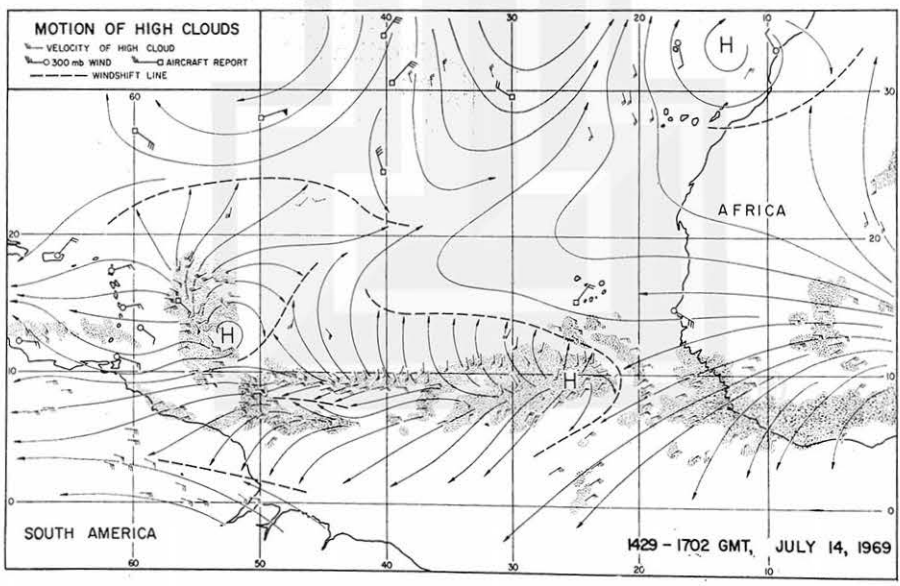

Fig. 6 Motion of high clouds computed from ATS III pictures taken between 1429–1702 Z, July 14, 1969.

the magnitude of convergence from measured cloud velocities. However, the existence of a shallow convergence layer along the west side of the thin line can reasonably be expected. A major convergence field which maintains the cloud clusters should be located directly beneath the clusters. Its identity has not been found in this case, because no cellar clouds were tracked between the thin line and the west edge of the clusters.

5. Velocity of high clouds

The velocities of high clouds presented in Fig. 6 clearly indicate that upper divergence fields are closely related to the locations of cloud clusters. There are two significant regions of upper divergence, one over cloud clusters east of Barbados and the other over a large cluster along 10N near 25W. Larger scale cloud-velocity patterns at high levels are completely modified by these diverging high clouds. The magnitude of cloud-velocity divergence in these two regions was estimated to be in the order of 10^{-4} per sec. Such patterns of velocity divergence seem to act as small scale blocking areas restricting environmental high clouds to move through the outer boundaries. As a result, a marked velocity shift lines are seen along the leading edges of high-cloud outflow from cloud cluster regions. Similar features of outflow were reported by Fujita, *et al.*, (1969), over the tropical Pacific.

6. Scatter diagram of cloud velocities

After determining the anticyclonic circulation center of cloud velocities at 34N and 37W, (surface anticyclone center at 33N and 35W) change in the velocities as a function of the distance from the center was studied. Five pie-shaped areas as shown in Fig. 7 were established so that cloud velocities in each sector could be plotted in a scatter diagram. The first sector was chosen in the direction of Africa, Sector II toward the opening between Africa and South America, Sector III toward eastern South America, Sector IV toward cloud clusters to the east of Barbados, and Sector V toward Puerto Rico.

As expected, cloud velocities which are zero at the anticyclone center increased rapidly toward Africa (see Fig. 8), reaching a maximum of about 17 kt mean motion. The range of velocity fluctuation between 14 and 20 kt is

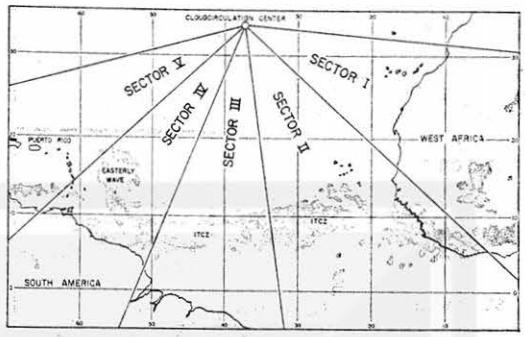

Fig. 7 Five pie-shaped sectors from the center of anticyclonic cloud motion.

due to both tracking error and natural variations within Sector I.

In Sector II, the velocities are available all the way to the equator. The scatter diagram in this sector, therefore, included velocities south of ITCZ. Fig. 8 clearly shows that the mean velocity reaching 22 kt half way between the anticyclone center and ITCZ decreased to only several knots inside the ITCZ. To the south of ITCZ, the speed increased to about 15 kt. Evaluation of Fig. 5 together with the scatter diagram reveals that the field of such cloud motion is a characteristic of convergent, cyclonic motion of low-level flow in and around an ITCZ.

Sector III covers an area of weak ITCZ where more scatter in cloud motion and insignificant velocity decrease were seen in the third diagram in Fig. 8.

The cloud-velocity cross section through an easterly wave in Sector IV indicated a significant speed drop of 13 kt in the eastern half of the cloud clusters inside the wave. Such a decrease combined with relatively straight flow inside the cluster region resulted in a field of convergence which traveled westward with the cloud clusters. In other words, the existence of the traveling convergence field maintained the cloud clusters which moved toward Barbados.

Inside Sector V, where no significant cloud clusters are in existence, the mean cloud-motion field showed little change. Scatter in speed on both sides of the mean values was about 5 kt.

Examination of five scatter diagrams in Fig. 8 implies that the large scatter in cloud motion is mainly due to the natural scatter resulting from mesoscale motion fields inside

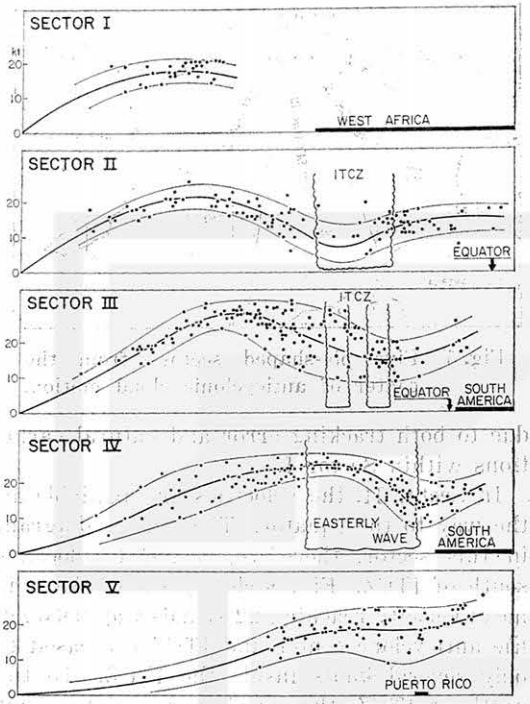

Fig. 8 Scatter diagrams of cloud speeds as a function of distance from the center in each of five sectors in Fig. 8. Upper and lower limits of cloud speeds are indicated by thin lines and average speeds by heavy line.

each of these 5 sectors. In the region of least natural scatter, one expects to find narrow ranges of variation in velocities. There are several such locations where dots distribute within a range of only 5 kt. If there were no natural mesoscale variations in cloud velocities, this 5 kt scatter should be regarded as a tracking error. In reality, however, a few knots variations due to mesoscale field of motion are always expected no matter where the locations are selected. Therefore, we may safely assume that the error of such a velocity computation is in the order of few knots, say 2 to 3 kt if careful computations of cloud velocity are performed.

7. Velocity of dust and wave clouds

An extensive tongue of a cloud of dust extending westward from Sahara was also analyzed. It was first assumed that the dust cloud was transported out from West Africa by relatively low-level winds. The velocities of low clouds just west of the coast, however, showed a northerly direction, making it very difficult to consider that dust can be transported westward while low clouds are moving southward. On the other hand, high clouds moving into the Atlantic from Africa were not coming from Sahara, thus ruling out the possibilities that dust clouds are carried up to the level of high clouds over Sahara.

Determination of dust velocities appeared to be an extremely difficult task because the patches of dust are not well defined. Moreover, apparent brightness patterns change significantly due to underlying low clouds and desert regions. To overcome difficulties in tracking dust patches, an attempt was made to speed up dust motion by selecting pictures at 30 to 40-min. intervals and by projecting them at 24 frames per second. It was found that this accelerated view provides an efficient way of dust-cloud tracking which is rather difficult otherwise.

As shown in Fig. 9, dust clouds were drifting straight west over the west coast of Africa north of Dakar. Upon traveling over 1000 km westward, the northern end of the dust cloud changed the direction of motion toward the north, then toward the east, drifting back toward Africa. The southern portion of the dust cloud kept traveling west at about 30 kt, thus extending the dust tongue far into the Atlantic toward Barbados and the West Indies after a few days.

Previously, the leading edge of a dust cloud leaving Africa on June 28, 1969 reached the longitude of Barbados about six days later. A 2400 n.m. travel distance in 6 days corresponds to an average speed of 400 n.m. per day or less than a 20 kt speed which is comparable but slower than the transport rate of dust clouds analyzed in Fig. 9. Although the height of the effective level of the dust transport cannot be determined from ATS pictures, the level when departing Africa is likely to be between the top of trade cumuli and high clouds.

Seen in the ATS III movie loops, in addition to the motion of the edge of the dust cloud, are long lines of waves with an amplitude of some 50 miles. As seen in Fig. 3, these waves extending SW-NE direction are identifiable. They appear, of course, more distinctly in a movie. These wave fronts are more or less parallel to the leading edge of the dust cloud but traveled northwest at the rate of about

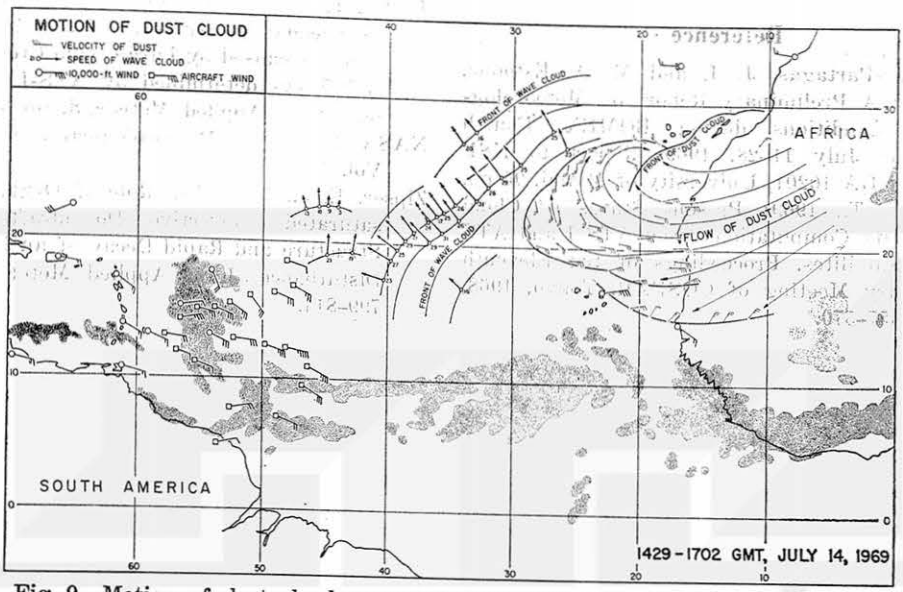

Fig. 9 Motion of dust cloud computed from ATS III pictures taken between 1429–1702 Z, July 14, 1969. Included in the picture are fronts of wave clouds propagating northwestward from the dust area.

25 kt. Velocity component of the dust front toward the northwest is considerably slower than 25 kt, suggesting that wave fronts created along the dust front propagated northwestward away from the dust area.

The interaction of the wave fronts and cellular trade cumuli is seen remarkably well in a loop movie used for this analysis. As the wave fronts moved over the trade cumuli, clouds increased in brightness and size. Between successive fronts, clouds became smaller and darker. The traveling waves, however, did not alter the motion of each cumulus cell despite the changes in brightness and size modulated by the passing waves.

Entered also in Fig. 9 are the 8,000-ft winds analyzed by Fernandes-Partagas and Estoque (1970) in their BOMEX data studies. Unfortunately the flight did not extend to the African coast for its possible use in the determination of the level of the dust cloud under discussion. Examination of Fig. 9 reveals, however, that a band of 8,000 ft maximum wind, assumed to be a "dust carrier band", was in existence between 10N and 15N over the flight area. This dust carrier band could be extended toward the leading edge of the dustflow located between 30W and 20W on July 14. The dust carrier band is likely to be in the middle level and varies its width and intensity as it moves across the Atlantic. We may expect also that internal gravity waves are created whenever velocity surge and/or sudden widening of the dust carrier band takes place.

8. Conclusions

A test analysis of both cloud and dust velocities over the northern tropical Atlantic Ocean revealed that the fields of cloud velocities obtained from successive ATS III pictures are very useful as additional data to past and future tropical experiments.

Although the movie technique provides a quick and accurate method of velocity determination, the picture intervals and total picture period must be selected differently for dust and cloud studies.

If we select cellular or well-defined clouds, our error of velocity computation should be within 3 kt of true cloud velocities.

It should be pointed out, however, that the determination or estimate of cloud height is one of the most important and difficult tasks. Although the results presented in this paper give velocities for at least two levels, their verification by using BOMEX and other synoptic data is of vital importance to the solution of cloud-height assignment problems.

Reference

Fernandez-Partagas, J. J. and M. A. Estoque, 1970: A Preliminary Report on Meteorological Conditions during BOMEX, Fourth Phase, July 11–28, 1969. Report to NSF under GA 10201, University of Miami, 95 pp.

Fujita, T. T., 1969: Present Status of Cloud Velocity Computations from ATS I and ATS III Satellites, Proceedings of the Eleventh Plenary Meeting of COSPAR, Tokyo, 1968, pp. 557–570.

Fujita, T. T., K. Watanabe, and T. Izawa, 1969: Formation and Structure of Equatorial Anticyclones caused by Large-scale Cross-equatorial Flows determined by ATS-I Photographs. J. of Applied Meteor. **8**, pp. 649–667.

NASA, 1969: ATS Meteorological Data Catalog, Vol. IV. GSFC.

Zipser, E. J., 1969: The Role of Organized Unsaturated Convective Downdrafts in the Structure and Rapid Decay of an Equatorial Disturbance, J. of Applied Meteor. **8**, pp. 799–814.